Hindawi
Geofluids
Volume 2021, Article ID 6561152, 8 pages
https://doi.org/10.1155/2021/6561152

Research Article

Identification of Initial Crack and Fracture Development Monitoring under Uniaxial Compression of Coal with High Bump Proneness

Zuoqing Bi, Han Liang, and Qianjia Hui

College of Mining Engineering, Liaoning Technical University, Fuxin 123000, China

Correspondence should be addressed to Han Liang; 18641822228@163.com

Received 5 August 2021; Accepted 30 November 2021; Published 21 December 2021

Academic Editor: Jia Lin

The rock burst proneness of coal is closely related to the coal mass structure. Therefore, the initial crack distribution of high burst proneness coal, its fracture development, and failure process under loading conditions are of great significance for the prediction of rock burst. In this study, high burst proneness coal is used to prepare experiment samples. The surface cracks of the samples are identified and recorded. The internal crack of the sample is detected by nuclear magnetic resonance (NMR) technology to determine the crack ratio of each sample. Then, 3D-CAD technology is used to restore the initial crack of the samples. Uniaxial compression test is carried out, and AE properties are recorded in the test. The stress-strain curve, the distribution of the fractural points within the sample at different stress states, and the relationship between ring count and stress are obtained. Results show that the stress-strain curves of high burst proneness coal are almost linear, to which the stress-ring count curves are similar. The distributions of fractural points in different bearing states show that the fracture points emerge in the later load stage and finally penetrate to form macrofracture, resulting in sample failure. This study reveals the initial crack distribution of coal with high burst proneness and the fracture development under bearing conditions, which provides a theoretical basis for the prediction technology of rock burst and technical support for the research of coal structure.

1. Introduction

Coal bump, or coal burst, is a type of violent geological disaster that is described by sudden and rapid destruction of coal mass around the roadway or a coal pillar, causing casualties and significant economic loss. Along with deep underground mining, coal bump has become a major disaster for major coal-producing countries. For example, as the biggest producer and consumer of coal in the world, China currently has 132 burst proneness coal mines with an average mining depth of 653 m [1].

There are many factors related to rock burst. Firstly, geological conditions, such as buried depth, faults, and folds, are closely related to rock burst [2, 3]. Horizontal tectonic stress is identified as the force source of rock burst [4–6]. Rock burst may also be related to gas and water contents and their migration [7–9]. Mining-related disturbances are also an important factor to inducing rock burst [10–13]. In addition, the property of coal and rock mass itself, that is, the so-called burst proneness, is another important factor in the occurrence of rock burst [14–17].

Coal is composed by matrix material and joints. Therefore, the impact tendency of coal is related to the structure of coal [18–20]. Regarding the research on the relationship between coal macrofracture and rock burst, Yin et al. [21] used CT technology to carry out uniaxial compressive test to analysis the CT of coal in each deformational stage from microcrack initiation, bifurcation, development, fracture, and failure. Pan et al. [22] analysed the energy storage and consumption of coal from the perspective of microstructure and constructed a quantitative relationship between the lithologic fabric of the coal and its impact tendency. Zhao et al. [23] used X-ray diffraction, SEM, and microphotometer to analyse the strength of coal burst proneness and obtained the relationship between coal internal mesostructural parameters and burst proneness. Jiang et al. [24] used

Table 1: Average physical and mechanical parameters of the coals.

Density (kg/m^3)	Compressive strength (MPa)	Tensile strength (MPa)	Cohesion (MPa)	Internal friction angle (°)	Elastic modulus (GPa)	Poisson ratio
1350	30.00	3.89	5.16	29.27	4.62	0.32

XRD, paramagnetic resonance, and SEM to obtain the structure of coal samples before and after rock burst and explored the characteristics of energy dissipation in the process of rock burst. Wu and Liu [25] studied the relationship between the pore development and the burst proneness of coal in the SEM image through the fractal method and proposed that the larger the fractal dimension is, the smaller the burst proneness is.

These studies show that the coal burst proneness is closely related to the coal structure. However, there are few methods to identify the initial cracks in coal body and to examine the fracture development under loading conditions, resulting in difficulties in the study of rock burst. In this study, the initial cracks of coal were identified by nuclear magnetic resonance (NMR) technology and represented by 3D-CAD technology. Acoustic emission (AE) technology is used to monitor the internal fracture point of coal under uniaxial compression, which is used to analyse the fracture development of the coal sample. This study provides a basis for the study of the relationship between coal structure and coal burst proneness and provides a technical support for coal burst prediction.

2. Materials and Methods

2.1. Sample Preparation. The coal samples studied in this paper were taken from Xinzhouyao Coal Mine, Datong, China. The average compressive strength of the coal samples is approximate 30 MPa with high bump proneness. Standard rock mechanics testing was conducted to measure the physical and mechanical parameters of the coals, including compressive, Brazilian tensile, varying angle shearing tests. The testing results of the samples are shown in Table 1.

For sample preparation, the coal blocks were cut by a cutting machine and then taken the core by a coring machine. Coal samples were finally processed into standard cylindrical specimens with dimensions of 50 mm (in diameter) × 100 mm (in length), as shown in Figure 1. Sample preparation was in accordance with the International Rock Mechanics Test Recommendation (IRTM) that the error of the parallelism depth between the upper and lower surfaces was within 0.02 mm. To assure the accuracy of the experiment, 9 coal specimens were prepared.

After sample preparation, the cracks in the sample surface were measured. The main cracks of each sample before testing are listed in Table 2.

2.2. Experiment Equipment

2.2.1. NMR. The NMR equipment is shown in Figure 2. The applied intensity of the magnetic field is 0.3-0.5 T, and the main frequency of the instrument is 12 MHz. To ensure that the sample is in the middle of the magnetic field, the coil diameter of the magnetic field was selected as 60 mm. The analysis equipment is a nuclear magnetic imaging software and a gradient pulse instrument. The imaging software can set the slice width, number of slices, and slice gap of the sample. After positioning, prescanning, formal scanning, and imaging of the sample, the crack structure inside the sample is displayed in the form of slices.

Figure 1: Prepared coal samples.

2.2.2. Loading Machine and AE Devices. WAW-600C computer-aided electrohydraulic servo universal testing machine is used to conduct the compressive test. AE monitoring device is simultaneously instrumented to observe the dynamic response of the specimen structure under uniaxial loading. The maximum loading capability is 600 kN, the measuring amplitude ranges from 2% to 100% of the maximum loads, the maximum piston rising velocity is 70 mm/min, the lifting velocity of the loading plate is 150 mm/min, the maximum piston stroke is 250 mm, and the maximum distance between the compression plates is 500 mm.

The AE technology is an effective method to detect the dynamic change of the material structure under the action of external loading through instrumentation. Each channel of the data acquisition system consists of measuring instrument, digital signal processor, computation program, and other peripheral apparatus, which are finally connected to a computer. The components of each channel include an AE sensor, a preamplifier, and a data acquisition card, as shown in Figure 3.

Table 2: The initial surface crack of each coal sample.

	Crack no.	Position (mm)	Direction	Length (mm)	Width (mm)	Thickness (mm)
1	1	Top 5.2	Horizontal	23.8	13.2	0.25
2	1	Bottom 12.3	Horizontal 30°	25.8	9.5	0.96
3	1	Bottom 38	Horizontal 45°	27.6	13.8	0.62
	2	Inclined	Vertical	25.3	19.3	0.78
4	1	Bottom 5	Horizontal	19.2	17	0.36
5	1	Top 45	Horizontal	33.1	16.4	0.40
	2	Top	Vertical	24.3	13.2	0.42
6	1	Top 55	Horizontal	19.5	17.9	1.00
	2	Top 50	Horizontal	27.4	16.3	0.3
	3	Top 10	Vertical	21.3	10.1	0.22
7	1	Top-middle	Vertical	38.3	15.3	0.1
8	1	Top-middle	Vertical	48.3	9.3	0.3
	2	Middle	Horizontal 80°	30.1	18.2	0.25
9	1	Bottom 10	Horizontal	26.3	16.1	0.5
	2	Bottom 20	Horizontal	28.4	15.0	0.5
	3	Bottom 35	Horizontal	23.4	21.5	0.52
	2	Bottom	Vertical	51.3	22.4	0.28
	3	Top 15	Horizontal	18.4	16.7	0.4
	4	Top 17	Vertical	23.4	8.4	0.23

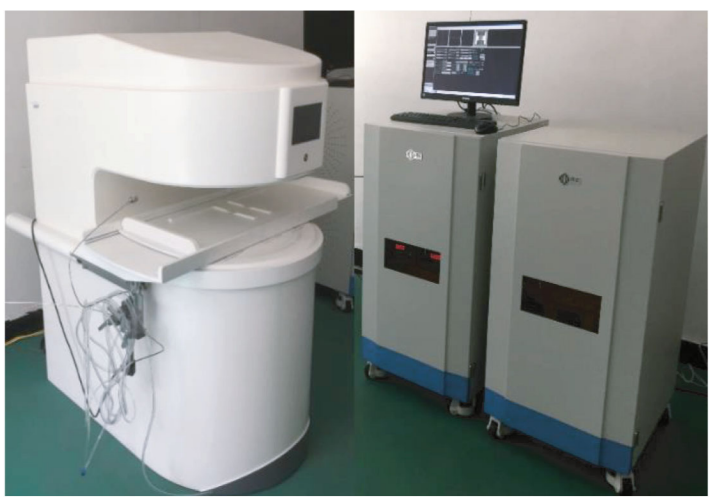

Figure 2: NMR instrument.

(a) AE sensor (b) Signal amplifier (c) Signal acquisition instrument (d) Signal analysis terminal

Figure 3: Acoustic emission signal transmission process.

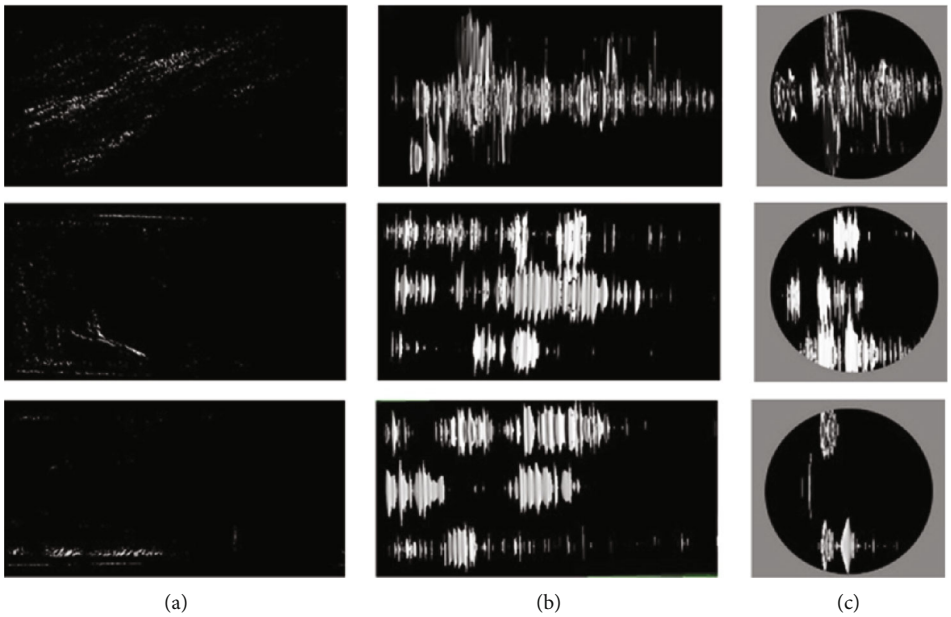

Figure 4: NMR reconstruction of coal samples: (a) main view, (b) top view, and (c) side view.

Figure 5: Testing procedure.

Table 3: Dimension and crack ratio of coal sample.

Sample no.	Diameter (mm)	Height (mm)	Crack ratio (%)
1	50.14	100.84	0.04
2	50.21	100.10	0.12
3	50.11	100.03	0.32
4	50.17	100.05	0.06
5	50.12	100.63	0.18
6	50.08	100.42	0.27
7	50.04	100.04	0.03
8	50.17	100.84	0.14
9	50.02	100.45	0.35

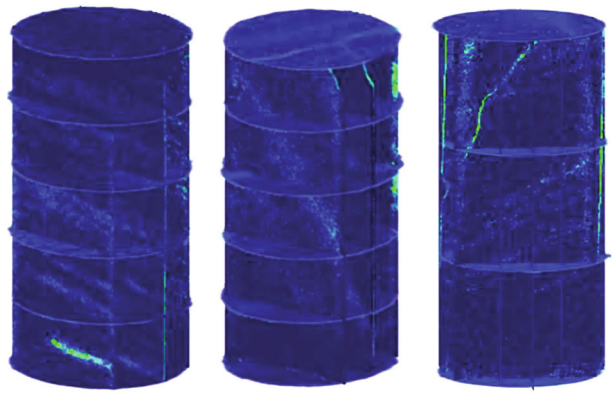

Figure 6: 3D-CAD sample reconstruction diagram.

2.3. Experimental Procedure

2.3.1. Initial Crack Identification Using NMR. The internal crack distribution of the sample can be obtained by processing the 3D slice map using NMR 3D reconstruction software. The NMR 3D reconstruction map of typical samples is shown in Figure 4, in which the white areas indicate the crack.

2.3.2. Uniaxial Compressive Test. The uniaxial compression testing system and the AE monitoring system are used to dynamically monitor the experimental data. The uniaxial compression testing machine is controlled by displacement with a loading rate of 0.5 mm/min. For parameters of the AE instrument, the threshold of the AE monitoring is set as 45 dB to minimize the effect of surrounding noises. The peak definition time (PDT), the hit definition time (HDT), and the hit locking time (HLT) are selected as 300, 600, and 1000 μs, respectively. The sound velocity is set to be 1.8 km/s.

After parameter setting was completed, fusing test was conducted on the specimen to verify the sensitivity of each

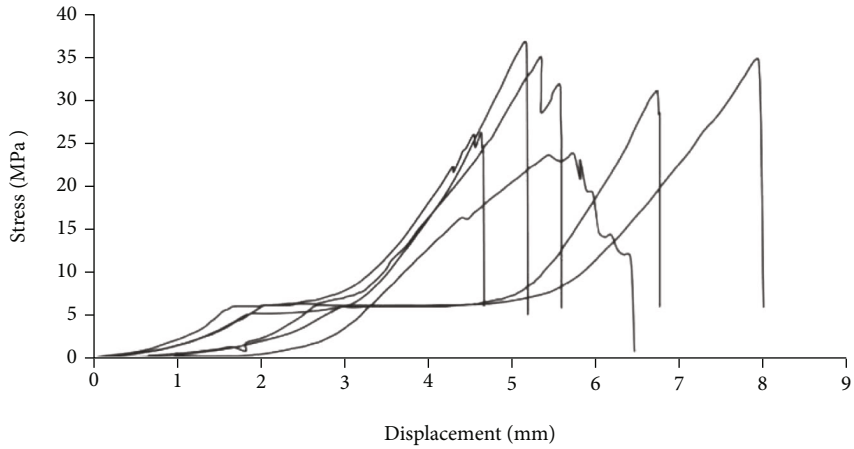

Figure 7: Stress-strain curves of testing sample.

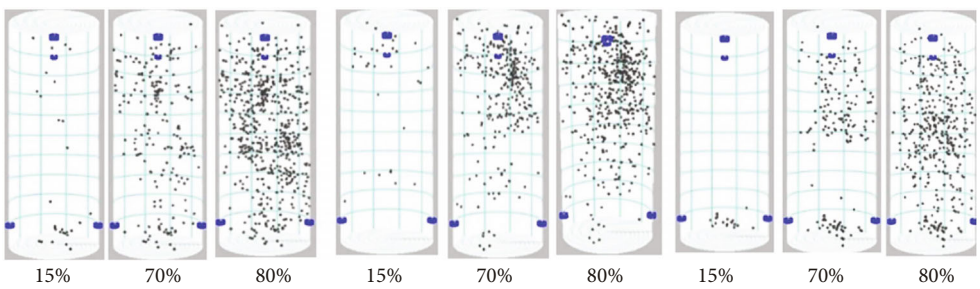

Figure 8: Distributions of the fractured sources of specimens 1-3.

sensor to guarantee the reliability of the experiment. Coupling agent needs be evenly pasted on the interface between the sensor and the testing sample for high-quality acquisition data. A piece of paper was placed between the testing machine and the specimen to eliminate friction. After the parameter setting and fusing testing are completed, uniaxial compression tests are carried out. The stress loading system and the AE monitoring system were turned on simultaneously. The experimental arrangement is shown in Figure 5.

3. Results and Discussion

3.1. Initial Crack Ratio. According to the NMR data, the initial crack ratio can be calculated. As the internal crack of the sample is an irregular body, to simplify the calculation, the internal crack of the sample is regarded as a regular cuboid, and the parameter index is length, width, and height. The crack ratio of each coal sample is shown in Table 3.

3.2. 3D-CAD Reconstruction of Initial Cracks. By import the 3D slice diagram of the sample into CAD software, the 3D-CAD reconstruction diagram of the initial cracks can be obtained. It provides a digital description for crack and fracture parameters, which can be used for fractural mechanism study and mesa-data analysis. Typical 3D-CAD crack reconstruction diagram of coal sample before testing is shown in Figure 6.

3.3. Results of Uniaxial Compression Tests. Figure 7 shows stress-strain curves of the testing samples. The deformational behaviour of hard coal shows a brittle property. After the compaction stage, the compressive stiffness of the coal is nearly uniform until sample failure.

3.4. AE Fracturing Point Distribution. The AE monitoring device identifies the locations of the fractured points in the coal specimen through sound waves released in the failing process of the specimen. Figure 8 shows the distributions of the wave sources at the stress levels of 15%, 70%, and 80% of peak stress of three testing samples.

Result shows that, along with increasing of axial load, the AE activities in the specimen increase, and the AE events are distributed nearly symmetrically along the central axis of the specimen. The AE events of the hard coal specimens are mainly concentrated near the central axis of the specimen, indicating there is a strong energy accumulation around the central axis. The AE events of the soft coal specimens are more sparsely distributed in the coal specimens and slightly concentrated near the middle part of the specimens.

3.5. AE Counts under Different Loading Conditions. AE count, also called ring count or ringdown count, refers to the number of times that the wave signals formed in AE beyond the threshold value. In this experiment, each wave signal exceeding the threshold is recorded as one AE count, which is regarded as one crack damage in the specimen. The

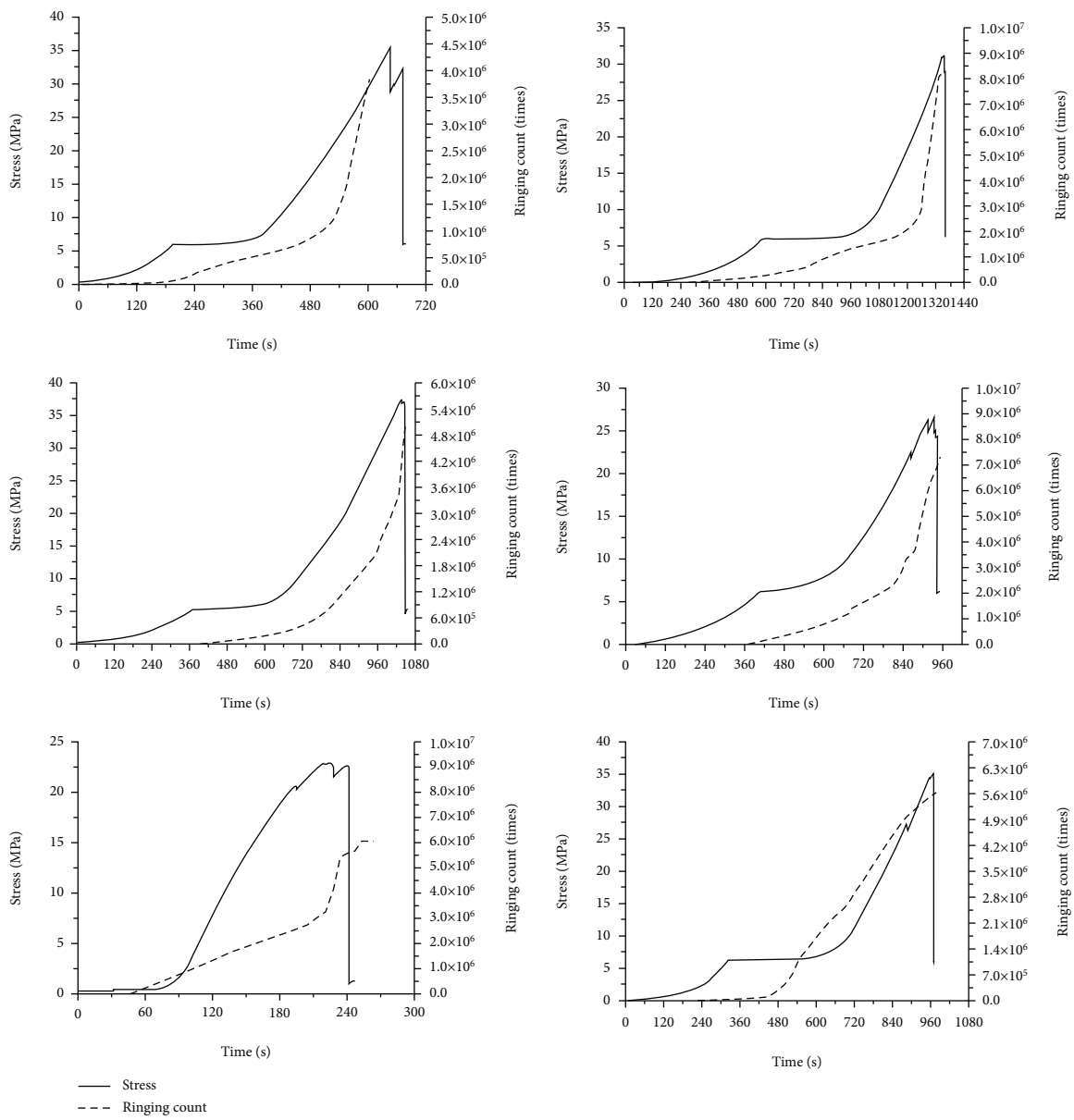

Figure 9: AE count results of specimens 1-6.

more AE counts suggest the more damage in the specimen at that moment. The number of the AE counts changes with time, as illustrated in Figure 9.

Result shows that the AE counts of the specimen appear in the early stage, and the maximum number is from 3.8×10^6 to 8.2×10^6 with average about 6.0×10^6. It suggests that the coal specimens with higher strength have a slow growth of the AE events at the early stage of the loading process. At the middle elastic stage, the fractured sources increase gradually, and at the end of the linear stage, the AE fractured points increase sharply.

4. Discussion

Traditionally, the deformation of coal under uniaxial compression is divided into the following five stages: compaction, elastic, elasto-plastic, strain-softening, and residual [26, 27]. In the compaction stage, the pore space and primary microcracks are compressed along with stress increasing. Elastic and elastoplastic stages are featured by linear relationship between the stress and strain. The specimen is compressed more tightly, and microcracks begin to develop within the specimen. In the strain softening stage, cracks propagate rapidly to form macrofracture. The peak stress is a point indicating failure of the coal sample along the main fracture. After peak, the deformation of the sample enters residual stage, in which the stress is residual strength of the coal.

For coal with high bump proneness, the testing result of this study suggests that, from the compaction to strain softening stage, the stress-strain curve is nearly linear, and the residual strength of the hard coal is close to zero rapidly. It suggests that such deformational behaviour is a feature for coal mass with high burst proneness.

AE event is often appeared in cluster model [28]. By comparing the fractured source locations at different stress levels, the testing result shows that, for hard coal, it has less AE events and when the loading stress is within the range of 10% to 20% of the peak stress. When the stress increases to 70%-80% of the peak value, the AE events became more active, suggesting rapid crack propagation in the coal specimen. After the stress reaches more than 80% of the peak stress, macrocracks propagate and expand rapidly and merge with each other, leading sudden failure of the specimen. It indicates that the AE events of hard coal increase slightly at the early stage of the compression. Then, it increases steadily in the linear elastic stage and increases sharply after linear elastic stage. Accordingly, the specimen undergoes primary crack coalescence, expansion, stable propagation, and ultimate macroscopic failure.

Combining the AE events with the deformational behaviour in the testing process, it suggests that, for hard coal, the cracks are developed in the later linear stage; that is, the AE counts comply with the growth of semiexponential function. The peak AE account of the coal specimen with high burst proneness takes place prepeak stress as the failure mode of the specimen is brittle; *i.e.*, there is nearly no energy that dissipates after the peak stress.

5. Conclusions

To study the structure of high burst proneness coal, NMR, 3D-CAD, and AE technology were used to identify the initial cracks and fracture development of coal samples under uniaxial compression condition. The following conclusions can be drawn.

(1) The initial crack in the sample is detected by NMR, and the crack ratio of each sample is obtained, which is a dominant factor on the bearing performance and deformation characteristics of the coal sample. By observing the surface cracks of the sample, the initial cracks can be restored by 3D-CAD

(2) The uniaxial compression test results show that the stress-strain curve of the sample has a remarkably high linearity, indicating that the coal with high burst proneness has the characteristic of brittleness

(3) In the process of uniaxial compression, the relationship between ring count and stress is obtained by using AE technology. The results show that the increase of ring count is consistent with the change of stress. Therefore, for coal with high burst proneness, the monitoring of ring counts is an effective means of stress analysis

(4) Through the analysis of fracture point distribution in different loading stages, it is considered that the fracture development of coal with high burst proneness is mainly concentrated in the later loading stage

This study reveals the initial crack distribution of coal with high burst proneness and the fracture development under bearing conditions, which provides a theoretical basis for the prediction technology of rock burst and technical support for the research of coal structure.

Data Availability

All data of this article has been included in this manuscript.

Conflicts of Interest

The authors declare that there is no conflict of interest regarding the publication of this paper.

Acknowledgments

This work was financially supported by the National Natural Science Fund of China (51774174).

References

[1] Q. X. Qi, Y. Z. Li, S. K. Zhao et al., "70 years development of coal mine rockburst in China: establishment and consideration of theory and technology system," *Coal Science and Technology*, vol. 47, no. 9, pp. 1–40, 2019.

[2] Y. Jiang and Y. Zhao, "Research status of coal mine rockburst in China: mechanism, early warning and control," *Journal of Rock Mechanics and Engineering*, vol. 34, pp. 2188–2204, 2015.

[3] K. Wang and F. Du, "Coal-gas compound dynamic disasters in China: a review," *Process Safety and Environmental Protection*, vol. 133, pp. 1–17, 2020.

[4] Q. X. Qi, T. Q. Liu, and Y. W. Shi, "Mechanism of friction sliding de-stability of rock burst," *Mine Pressure and Roof Management*, vol. Z1, 1995.

[5] S. Wang, D. Li, C. Li, C. Zhang, and Y. Zhang, "Thermal radiation characteristics of stress evolution of a circular tunnel excavation under different confining pressures," *Tunnelling and Underground Space Technology*, vol. 78, pp. 76–83, 2018.

[6] J. Han, H. Liang, C. Cao, Z. Bi, and Z. Zhu, "A mechanical model for sheared joints based on Mohr-Coulomb material properties," *Géotechnique Letters*, vol. 8, no. 2, pp. 92–96, 2018.

[7] L. Zhang, J. H. Li, J. H. Xue, C. Zhang, and X. Fang, "Experimental studies on the changing characteristics of the gas flow capacity on bituminous coal in CO_2-ECBM and N_2-ECBM," *Fuel*, vol. 291, article 120115, 2021.

[8] J. Lin, T. Ren, G. Wang, P. Booth, and J. Nemcik, "Experimental investigation of N_2 injection to enhance gas drainage in CO_2-rich low permeable seam," *Fuel*, vol. 215, pp. 665–674, 2018.

[9] J. Lin, T. Ren, Y. P. Cheng, J. Nemcik, and G. Wang, "Cyclic N_2 injection for enhanced coal seam gas recovery: a laboratory study," *Energy*, vol. 188, article 116115, 2019.

[10] L. Dou and Z. Mu, *Rockburst Prevention and Control of Coal Mine*, Science Press, Beijing, China, 2018.

[11] D. J. Xue, J. Wang, Y. Zhao, and H. Zhou, "Quantitative determination of mining-induced discontinuous stress drop in coal," *International Journal of Rock Mechanics and Mining Sciences*, vol. 111, pp. 1–11, 2018.

[12] Q. Qingxin, C. Shangben, W. Huaixin, M. Debing, and W. Yongxiu, "Study on relations among coal bump, rockburst and mining tremor with numerical simulation," *Chinese Journal of Rock Mechanics and Engineering*, vol. 11, pp. 1852–1858, 2003.

[13] D. J. Xue, Y. T. Liu, H. W. Zhou, J. Q. Wang, J. F. Liu, and J. Zhou, "Fractal characterization on anisotropy and fractal reconstruction of rough surface of granite under orthogonal shear," *Rock Mechanics and Rock Engineering*, vol. 53, no. 3, pp. 1225–1242, 2020.

[14] Y. Jiang, Y. Pan, and F. Jiang, "State of the art review on mechanism and prevention of rock bumps in China," *Journal of China Coal Society*, vol. 39, no. 2, pp. 205–213, 2014.

[15] W. Liu, Y. Jiang, H. Zhou, and Z. H. Chen, "Experimental study on outburst proneness coal seam of meso character and crack destabilization," *Journal of Hunan University of Science & Technology*, vol. 21, no. 4, pp. 14–18, 2006.

[16] F. Jiang, Q. Wei, and S. Yao, "Key theory and technical analysis on mine pressure bumping prevention and control," *Coal Science and Technology*, vol. 41, no. 6, pp. 6–9, 2013.

[17] Z. C. Feng and Y. S. Zhao, "Correlativity of rock inhomogeneity and rock burst trend," *Chinese Journal of Rock Mechanics and Engineering*, vol. 22, no. 11, pp. 1863–1865, 2003.

[18] F. du, K. Wang, X. Zhang, C. Xin, L. Shu, and G. Wang, "Experimental study of coal-gas outburst: insights from coal-rock structure, gas pressure and adsorptivity," *Natural Resources Research*, vol. 29, no. 4, pp. 2481–2493, 2020.

[19] L. Zhang, S. Chen, C. Zhang, X. Fang, and S. Li, "The characterization of bituminous coal microstructure and permeability by liquid nitrogen fracturing based on μCT technology," *Fuel*, vol. 262, article 116635, 2020.

[20] Y. X. Zhao, Y. D. Jiang, and S. P. Tian, "Investigation on the characteristics of energy dissipation in the preparation process of coal bumps," *Journal of China Coal Society*, vol. 35, no. 12, pp. 1979–1983, 2010.

[21] G. Z. Yin, G. F. Dai, W. L. Pi, and D. W. Li, "CT experiment of coal rock damage evolution law under uniaxial compression load," *Chongqing University Journal*, vol. 26, no. 6, pp. 96–100, 2003.

[22] J. N. Pan, Z. P. Meng, and B. M. Liu, "Relationship between rock composition and texture of coal-bearing formation and its burst potential," *Chinese Journal of Rock Mechanics and Engineering*, vol. 24, no. 24, pp. 4422–4427, 2005.

[23] Y. X. Zhao, Y. D. Jiang, and Y. Zhang, "The relationship between bump-prone properity and microstructure characteristics of coal," *Journal of China Coal Society*, vol. 32, no. 1, pp. 64–68, 2007.

[24] Y. Jiang, Y. Lu, Y. Zhao, Y. Song, and L. Tao, "Multiparameter monitoring experiments for instability destruction of coal samples," *Chinese Journal of Rock Mechanics and Engineering*, vol. 31, no. 4, pp. 667–674, 2012.

[25] X. Wu and C. W. Liu, "Evaluation of impact tendency of coal rock based on surface fractal features," *Underground Space and Engineering*, vol. 9, no. 5, pp. 1045–1049, 2013.

[26] F. Du and K. Wang, "Unstable failure of gas-bearing coal-rock combination bodies: insights from physical experiments and numerical simulations," *Process Safety and Environmental Protection*, vol. 129, pp. 264–279, 2019.

[27] L. Xue-wei, L. Quan-sheng, C. Yuan, and L. Qiang, "Experimental study of effects of fracture type on strength characteristic and failure modes of fractured rockmass," *Rock and Soil Mechanics*, vol. 36, no. S2, pp. 208–214, 2015.

[28] D. Xue, L. Lu, J. Zhou, L. Lu, and Y. Liu, "Cluster modeling of the short-range correlation of acoustically emitted scattering signals," *International Journal of Coal Science & Technology*, vol. 8, pp. 1–15, 2021.